Metrol. Meas. Syst., Vol. XXI (2014), No. 2, pp. 317–328.

METROLOGY AND MEASUREMENT SYSTEMS

Index 330930, ISSN 0860-8229

www.metrology.pg.gda.pl

AUTOMATIC CALIBRATION SYSTEM FOR DIGITAL-DISPLAY VIBROMETERS BASED ON MACHINE VISION

Wen He[1)] , Guanhua Xu[1)], Zuochao Rong[2)], Gen Li[3)] , Min Liu[4)]

1) The State Key Laboratory of Fluid Power Transmission and Control, Zhejiang Province Key Laboratory of Advanced Manufacturing Technology, Zhejiang University, 310027, Hangzhou, China (✉ hewens@zju.edu.cn, +86-571-87952627)
2) Shanghai Key Laboratory of Spacecraft Mechanism, Shanghai 201109, China
3) ACRE Coking & Refractory Engineering Consulting Corporation, MCC, Dalian 116085, China
4) Zhejiang Provincial Institute of Electric Power Test and Research, 310014, Hangzhou, China

Abstract

Considering the low efficiency during the process of traditional calibration for digital-display vibrometers, an automatic calibration system for vibrometers based on machine vision is developed. First, an automatic vibration control system is established on the basis of a personal computer, and the output of a vibration exciter on which a digital-display vibrometer to be calibrated is installed, is automatically adjusted to vibrate at a preset vibration level and a preset frequency. Then the display of the vibrometer is captured by a digital camera and identified by means of image recognition. According to the vibration level of the exciter measured by a laser interferometer and the recognized display of the vibrometer, the properties of the vibrometer are calculated and output by the computer. Image recognition algorithms for the display of the vibrometer with a high recognition rate are presented, and the recognition for vibrating digits and alternating digits is especially analyzed in detail. Experimental results on the built-up system show that the prposed image recognition methods are very effective and the system could liberate operators from boring and intense calibration work for digital-display vibrometers.

Keywords: Image recognition, calibration, vibration measurement, machine vision, automatic testing, digital-display vibrometer.

1. Introduction

Digital-display vibrometers are widely applied in monitoring and fault diagnosis of industrial equipment due to their low energy consumption, high precision, great reliability, and portability [1-4]. To make all these vibrometers work well, their performance index should be calibrated periodically according to the corresponding metrological regulations like the ordinary vibration pick-ups [5-6]. When calibrating a vibrometer, an operator first installs its sensing head on the vibration table of a vibration exciter and makes the vibration exciter vibrate at a preset vibration level and a preset frequency, then reads and records the display of the vibrometer with naked eyes, and finally calculates the deviation between the display value and the vibration level manually. The whole calibration work is always done at different frequencies and vibration levels, so this conventional calibration process for digital-display vibrometers is terribly cumbersome. Since thousands of the vibrometers should be calibrated every year, it has become a heavy task for the corresponding metrological station.

An automatic calibration system for vibration pick-ups can free the operator from repetitive and boring work [7]. Most of the digital-display vibrometers could not be calibrated by the ordinary automatic calibration system directly because of no output or interface except the display on the vibrometers for cost considerations. In the recent years, machine vision technology has widely been applied in automatic systems [8-17]. A digital

Article history: received on Sep. 09, 2013; accepted on Feb. 08, 2014; available online on May. 15, 2014; DOI: 10.2478/mms-2014-0027.

camera can be applied to replace human eyes to capture the images of digital or analog displays, and then the captured images are transmitted to a computer, in which the displays are recognized by some image recognition algorithms. As for the recognition of the digital display, F.C. Alegria and A.C. Serra developed an automatic calibration system for analog and digital measuring instruments using computer vision [11, 12]. E. Vázquez-Fernández et al. proposed a complementary method with human perception for digit recognition [13], which was applied to calibrate digital thermometers [14]. P.A. Belan and S.A. Araujo et al. proposed a segmentation-free algorithm based on template matching to read the digital display [15].

Although a lot of recognition algorithms has been presented, their recognition rate [13, 14] does not meet the rigorous demand for the calibration as expected. Besides, recognition of the decimal point has not been considered in many studies [11, 12, 15]. Furthermore, a large number of digital-display vibrometers to be calibrated should be installed on the vibration table of a vibration exciter since their sensing heads and displays are integrated together into a package, thus the display values may be vibrating during calibrating at a frequency as high as 160Hz, which will result in a blurry image and lower recognition rate because of the limited acquisition speed of the camera. How to recognize the vibrating digits is an urgent problem to be solved in this case, which has not been mentioned in the existing literatures. Meanwhile, the displayed value on a vibrometer might alternate during the measurement, especially the last bit of the digits, which will result in erroneous recognition [14]. But the existing literatures have also not discussed how to solve the problem.

In this paper, an automatic calibration system for digital-display vibrometers is presented. Several programmable instruments are connected together with a computer to control a vibration exciter to vibrate at a preset vibration level and a preset frequency automatically. A digital camera is used to capture the display of the vibrometer to be calibrated. Some image recognition methods are put forward to recognize the captured images of the digital-display, which could solve the key problems for recognition of segmented-digits on the vibrometers.

2. Automatic calibration system

As a conventional calibration system for vibration pick-ups [18], the system consists of a vibration exciter, a power amplifier, a laser interferometer, a signal generator and a ratio counter, etc. In addition, our system includes a personal computer (PC), a digital camera and a set of corresponding computer interfaces such as Universal Serial Bus (USB) and General Purpose Interface Bus (GPIB), whose scheme is shown in Fig. 1. The vibrometer to be calibrated is installed on the vibration table. The ratio counter and the signal generator communicate with the PC through GPIB, while the camera communicates with the PC through USB. The signal generator outputs a sinusoidal signal whose frequency and amplitude are controlled by the PC. The signal is amplified by the power amplifier to drive the vibration exciter. The ratio counter measures the frequency ratio between the signals from the laser interferometer and the generator, and transmits the measured value to the PC, where it could be transformed to the vibration level of the exciter by the fringe counting method [7, 18]. Then the vibration exciter is controlled by the PC to vibrate at a preset vibration level and frequency. The display of the vibrometer is captured by the digital camera and transmitted to the PC. The images are transformed into numerical values by the specially-designed algorithm in the calibration software. According to the actual vibration level from the laser interferometer and the value displayed on the vibrometer, the technical performance of the vibrometer could be obtained.

The calibration software is the core of the system, which is responsible for control of the vibration exciter, image recognition, calculation, filing, printing, etc. The software is

programmed with LabVIEW, which is a graphical software system for developing high-efficiency scientific and engineering applications.

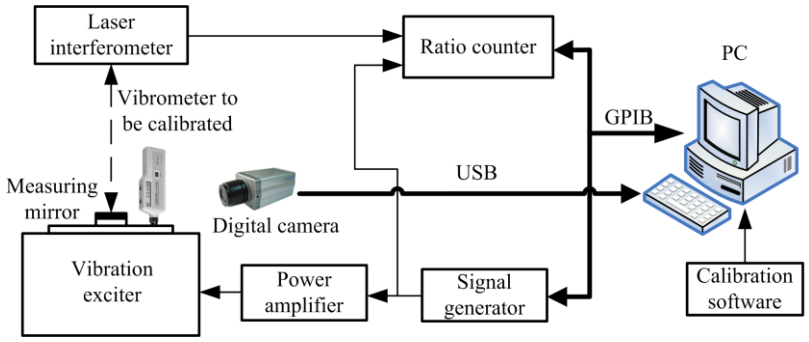

Fig. 1. Scheme of the automatic calibration system.

3. Image recognition

After the display of a vibrometer is captured by the digital camera, a region of interest (ROI) is drawn by an operator manually, which only covers the display value in the image. Aiming at the segmented digits in the ROI, which are common displays on the vibrometer, a group of image recognition algorithms are designed. The image pre-processings, such as image rotation, image grayscale, filter and binarization, have been well studied [19], so it is easy to get the pre-processed images, which are vertical and binarized digits images as shown in Fig. 2(a). Here methods of recognition for segmented-digits based on their morphologic characteristics are put forward, which helps to improve the recognition rate of digits. The recognition methods for vibrating digits and alternating digits are especially studied.

3.1. Stroke correction

For aesthetic reasons, the upright strokes of segmented-digits usually have a certain slant to the right as shown in light color in Fig. 3, which will influence the image recognition. So it is necessary to make every stroke in the digits vertical.

Assume that the captured image has been binarized and the pixel of the image is $\{g(i, j), 0 \le i \le w-1, 0 \le j \le h-1\}$, where i and j represent the column and row number respectively, w and h represent the width and height of the image respectively, $g(i, j) = 1$ when the pixel is highlighted and $g(i, j) = 0$ when the pixel is dark, and the coordinate origin is set at the upper left corner of the image.

(a) Original image (b) Stroke-corrected image (c) Division of characters

Fig. 2. Process of stroke correction and division.

Take the image of the digit 2 for an example, as shown in Fig. 3. Suppose that the correct angle per step is 0.5° and the maximum adjusting angle of strokes is $\alpha_{\max}$. Let the pixels in row j move round[$\tan(\alpha_n) \cdot j$] pixels rightwards, where the correction angle $\alpha_n = n \times 0.5°$, n is the step number of the transformation, and round[$\tan(\alpha_n) \cdot j$] is the function to find an

integer nearest to $\tan(\alpha_n)\cdot j$. The maximum of n is assumed as $n_{\max}$ which depends on $\alpha_{\max}/0.5°$. The pixels moved out of the right border will be deleted, while the pixels moved in from the left are set to 0. The transformation formula is

$$r(i,j)_n=\begin{cases}0, & 0\le i<\text{round}[\tan(\alpha_n)\cdot j],\\ \text{g}(i-\text{round}[\tan(\alpha_n)\cdot j],j), & \text{round}[\tan(\alpha_n)\cdot j]\le i\le w-1.\end{cases} \quad (1)$$

Then the projection of the transformed image onto the i axis, which is also called vertical projection, is calculated as

$$R(i)_n=\sum_{j=0}^{h-1} r(i,j)_n, \quad (2)$$

whose variance is

$$D_n=\frac{1}{w}\sum_{i=0}^{w-1}[R(i)_n-\frac{1}{w}\sum_{i=0}^{w-1}R(i)_n]^2=\frac{1}{w}\sum_{i=0}^{w-1}[R(i)_n-\bar{R}]^2. \quad (3)$$

As we know, $\bar{R}$ is the average value of the vertical projection, which is independent on n. As the slant angle of the digit decreases, the individual differences between $R(i)_n$ and $\bar{R}$ increase and D_n becomes larger. When D_n reaches its maximum as n changes from 0 to $n_{\max}$, all the strokes are vertical [20]. The original and stroke-corrected images are shown in Fig. 2(a) and (b), respectively.

3.2. Recognition of segmented digits

In the ROI, there are several digits and a decimal point, which are waiting to be recognized and should be separated one by one before recognition. As there are spaces between the straight characters, the vertical projection is adopted to separate the characters from each other [21]. Then the horizontal projection, which is the projection of the transformed image onto the j axis, is applied to remove the black regions above and below each character. Therefore, a group of single character images are obtained as shown in Fig. 2(c), each of which only contains a single character. Here a recognition method based on morphology is presented as follows.

There are 11 characters to be indentified in total, namely digits 0-9 and a decimal point. Assume that the maximum width and height in the images of a single character to be recognized are max_width and max_height, and the ratio range of max_height to max_width is from 1.8 to 3.2 according to the routine display. Since the height of each character to be identified is equal to max_height except the decimal point, it is easy to get max_height after a group of single character images have been obtained as shown in Fig. 2(c), and max_width can coarsely be estimated from the minimum ratio of max_height to max_width. The characters to be identified are divided into 3 classes based on width and height of the single character image.

(a) Decimal point. If the height of the single character image is less than 30% of max_height and its width is less than 50% of max_width and its position is at the lower part of the whole character image, it is considered to be a decimal point.

(b) Digit 1. If the width of the single character image is less than 30% of its height, it is considered to be digit 1.

(c) Digit 0 and 2-9. The characters that are not classified as above two characters are merged into this case. According to the morphologic characteristics of digit 0 and 2-9, the width and height of the character to be identified is almost equal to max_width and max_height. Otherwise, the character will be marked as an error character. As we know, a segmented digit includes 7 strokes, which define what the digit is. It is easy to determine the probable position where the centre of each stroke locates after the maximum width and height of the character to be identified are known. Seven small squares are defined, which are marked by a, b, c, d, e, f, and g as shown in Fig. 4. The centre of every square is defined at the centre of the stroke that it belongs to, and the side length of the square is just less than the width of the stroke which it belongs to, and there is no interference between the square and its neighboring strokes. During identification, if there are more than 30% highlighted pixels in the square, the flag of the square is set to 1; otherwise the flag of the square is set to 0. At last, the value of the digit could be identified by the flag values of each square in the image, as shown in Table 1.

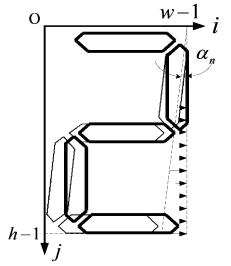

Fig. 3. Corrected strokes.

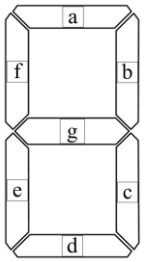

Fig. 4. Coded strokes.

Table 1. Relationship between the flag values and strokes.

Value	a	b	c	d	e	f	g
2	1	1	0	1	1	0	1
3	1	1	1	1	0	0	1
4	0	1	1	0	0	1	1
5	1	0	1	1	0	1	1
6	1	0	1	1	1	1	1
7	1	1	1	0	0	0	0
8	1	1	1	1	1	1	1
9	1	1	1	1	0	1	1
0	1	1	1	1	1	1	0

If the characters to be identified do not belong to any of the three classes listed above, it will be marked as an error character. In addition, only one decimal point could be recognized in one display. Otherwise, either of them will be marked as an error character. After all the single character images are identified, the display value of the vibrometer can be obtained based on the position of the decimal point. In order to improve the recognition rate, several continuous images for the display value of the vibrometer are captured and recognized respectively, and the value that has the most occurrences is the final correct result, which will be introduced in section 3.4.

3.3. Recognition of vibrating digits

The displacement of a vibrometer, which is installed on the vibration exciter during calibration, is assumed as

$$x(t) = A\sin(2\pi ft)\,, \tag{4}$$

where A is the displacement amplitude of the vibration table and f is the vibration frequency. Considering the mounting position of the vibrometers, the direction of the vibration is assumed to be consistent with the *i* axis of the image coordinates. Due to the limited acquisition speed of the camera, it is impossible to capture the theoretical instantaneous image actually. Only a blurry image in a period of record time could be got if f is too high. When the blurry area is so large that it will overrun the ROI border or the adjacent blurry edges will overlap each other, especially the edges of the digit and its nearby decimal point (because they are too close), it will be difficult to divide characters from each other. Therefore, the recognition accuracy will be affected.

To solve the problem, the maximum displacement amplitude $A_{\max}$ output from the vibration exciter at a specified frequency f should be limited considering the acquisition speed n (unit: frame per second) of the camera, the minimum distance a between ROI border and the stroke of the characters to be identified, and the minimum distance l between the strokes of the characters to be identified.

As shown in Fig. 5, the dashed part is the acquired blurry area due to the sampling period $T=1/n$ of the camera, and δ_1 and δ_2 represent the blurry border width of two adjacent strokes respectively, and Δ represents the actual gap of two adjacent strokes, whose gap is l when the strokes stand still. Two cases are discussed as follows.

(a) The sampling period for one image is not less than half of a vibration period, that is to say, $f \geq n/2$. In this case, the blurry edge of two adjacent strokes can reach its maximum width in the meantime, that is

$$\delta_{1\max} = \delta_{2\max} = A, \tag{5}$$

and the actual gap Δ of two adjacent strokes gets its minimum as

$$\Delta_{\min} = l - \delta_{1\max} - \delta_{2\max} = l - 2A. \tag{6}$$

(b) The sampling period for one image is less than half of a vibration period, that is to say, $f < n/2$. Assume that the time during blurry border width δ_1 is t_1, thus the time during blurry border width δ_2 is $T - t_1$. So the actual gap Δ of two adjacent strokes is

$$\Delta = l - [A\sin 2\pi f t_1 + A\sin 2\pi f (T - t_1)] = l - 2A\sin \pi f T \cos 2\pi f (t_1 - T/2). \tag{7}$$

So it is easy to find the minimum of Δ when $t_1 = T/2$, that is

$$\Delta_{\min} = l - 2A\sin \pi f T = l - 2A\sin \frac{\pi f}{n}. \tag{8}$$

In order to ensure the recognition accuracy, there should be $\Delta_{\min} > 0$. So the displacement amplitude A output from the vibration exciter at a specified frequency f should be limited as

$$\begin{cases} A < \dfrac{l}{2\sin(\dfrac{\pi f}{n})}, & f < \dfrac{n}{2}, \\ A < \dfrac{l}{2}, & f \geq \dfrac{n}{2}. \end{cases} \tag{9}$$

In addition, each stroke of the digit to be identified should not go out of the ROI border, so there should be

$$A \le a\,. \tag{10}$$

In brief, the relationship between the permissible amplitude A and frequency f, at which the vibration exciter could output, is drawn in Fig. 6. The recognition accuracy will not be affected only when the displacement amplitude output from the vibration exciter is not beyond the area of the section line, and the upper boundary of the area is the permissible maximum displacement amplitude $A_{\max}$ from the vibration exciter at the corresponding frequency. If the amplitude is confined to the permissible range at a specified frequency, we can ensure that all the characters can be captured without overlapping each other. Consequently, all the characters can be separated from each other and recognized after all the small squares in Fig. 4 are detected correctly.

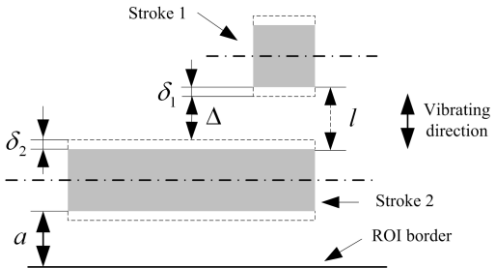

Fig. 5. Vibrating image.

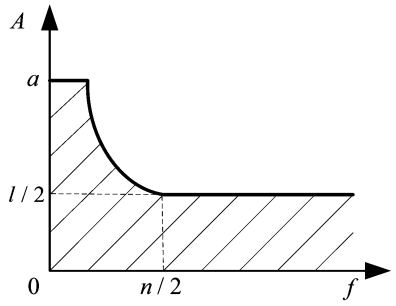

Fig. 6. Relationship between the permissible vibration amplitude and frequency.

3.4. Recognition of alternating digits

Due to the resolution of the digital instrument, the digital-display may change from one value to another although the vibration level of the exciter is stable, especially when the last character of the display is "9" or "0". The alternating digits will make the image confused as shown in Fig. 7, where the display is varying between 1.89 and 1.90. This will result in a recognition error [14].

Fig. 7. Display in transition.

In order to get the correct result, the continuous images (for example m images) in a relatively long period (sampling time) are captured and saved in the memory temporarily.

Assume that the display digit is alternating between X and Y, whose steady time is α_1 and α_2 respectively and the transition time is β. Notice that α_1 and α_2 are larger than β, that is

$$\alpha_1 > \beta \text{ and } \alpha_2 > \beta\,, \tag{11}$$

which is easy to be found with our naked eyes. Consider that the sampling period T of the camera could be much shorter than the transition time β with the help of a high-quality digital camera. And assume that p_0, q_0 and r_0 are the number of images which have been acquired in the time of α_1, α_2 and β, respectively. According to (11), there are

$$p_0 > r_0 \text{ and } q_0 > r_0 . \tag{12}$$

Assume that the sampling time is so long that m could satisfy

$$\alpha_1 + \alpha_2 + \beta < mT \tag{13}$$

or

$$p_0 + q_0 + r_0 < m . \tag{14}$$

In the m sampled images that satisfy (14), assume p, q and r are the numbers of occurring X, Y and others, that is

$$p + q + r = m . \tag{15}$$

Considering the difference between $p+q$ and r, it is found that the minimum difference $\eta_{\min}$ happens when $p = p_0$, $q = q_0$ and $r = 2r_0$, which is shown in Fig. 8, that is

$$\eta_{\min} = (p+q) - r = (p_0 + q_0) - 2r_0 . \tag{16}$$

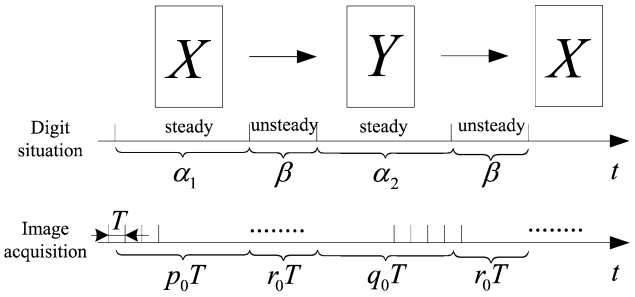

Fig. 8. Display in transition and image acquisition.

As mentioned above, the values of X and Y are very close, whose difference is just one display resolution, so X and Y could be regarded as the same value. Due to (12) and (16), there is $\eta_{\min} > 0$. Thus, in the m acquired images, the occurrences of X and Y ($p+q$) are more than those of others (r). So the identified value with the maximum number of occurrences (either X or Y) is definitely the correct final result.

4. Experimental results

The VM-63A vibrometer made by Rion, which is a typical digital-display vibrometer, is selected to test the built-up automatic calibration system.

First, the vibrometer is installed on the table of the exciter as shown in Fig. 9 because its sensing head is packaged with the display. In the figure, a universal magnetic base is used as a support for carrying and adjusting the camera, and a clamp is used to push the "measure" button on the vibrometer and make it work in the calibration process.

The vibrometer could be set to measure displacement, velocity, and acceleration by pressing three buttons, respectively. The non-linearity and frequency response should be calibrated according to the corresponding metrological regulations [6]. Here the velocity non-linearity at 40 Hz and the displacement frequency response at 50 μm (Peak to Peak) of the vibrometer are tested as an illustration. According to the measuring range of the vibrometer, the maximum vibration levels and corresponding maximum displacements are listed in Table 2. According to the properties of the digital camera, the characteristics of the digital-display on the vibrometer and the selected ROI, there are $n = 30$ fps, $l = 1$ mm,

$a = 1$ mm. According to (9) and (10), the permissible maximum amplitudes of the exciter at different frequencies are calculated and shown in Table 2, which indicate that they are always much larger than the corresponding maximum displacements of the vibration exciter, so the vibration will not affect the recognition accuracy according to the analysis in section 3.4.

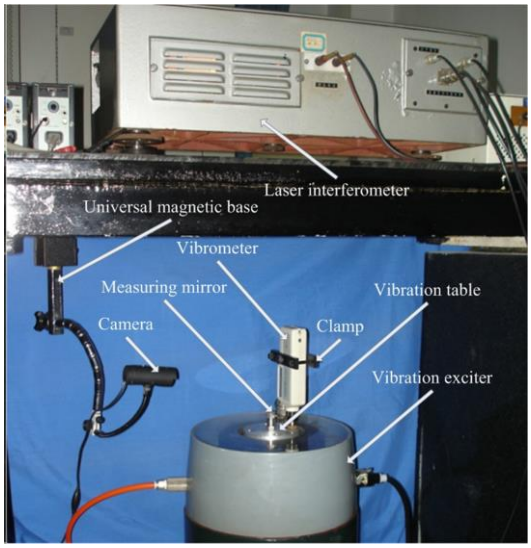

Fig. 9. Installation of the vibrometer to be calibrated.

Table 2. Test parameters and permissible maximum amplitude.

Test items	f (Hz)	Maximum vibration level	Maximum displacement $(\text{mm})_{0\text{-P}}$	Permissible maximum displacement $(\text{mm})_{0\text{-P}}$
Non-linearity	40	$30(\text{mm/s})_{\text{RMS}}$	0.169	0.5
Frequency response	10-160	$50(\mu\text{m})_{\text{P-P}}$	0.025	0.5 $(f > 15\text{Hz})$ $\frac{1}{2\sin(\pi f / 30)}$ $(10\text{Hz} \le f < 15\text{Hz})$

When the calibration software is started, some preparing work should first be done, in which ROI selection is an important job before calibration. The operation interface of ROI selection is shown in Fig. 10. The ROI is manually set by a green frame as shown in the figure. The pose of the camera and the illuminance on the display of the vibrometer are adjusted so that the recognition result is ensured to be correct all the time when pushing the "test" button on the interface. The operation interface for testing the velocity non-linearity of the vibrometer is shown in Fig. 11. The typical calibration results, which respectively represent the velocity non-linearity and displacement frequency response, are presented in Table 3 and 4. "Standard" in the tables stands for the actual vibration level measured by a laser interferometer, while "Display" stands for the recognition value of the vibrometer from our developed algorithms, where the values outside of brackets are the recognition results and the values in the brackets, which actually do not exist on the operation interface, are the actual display values read by our naked eyes. "Deviation" shows the calibration results for the vibrometer, which is the absolute value of the relative deviation between "Standard" and "Display" and will be given in the final certificate of the calibrated vibrometer. It is proved that the recognition result is definitely the same as the actual value. Moreover, hundreds of images were acquired and tested, and the recognition results were checked artificially. Results show that only 2 recognition errors occur in 800 recognized images, which proves that the recognition rate is about 99.75%. Further analysis shows that the errors are caused by

the disturbance of reflected light on the display panel. To avoid the recognition error due to the contingency, the operator is alarmed if a recognition error happens or an accident datum is recognized so that the deviation of the vibrometer has exceeded a preset value, and then the test will be done again from this point after checking the system artificially. This procedure is very important because recognition errors are not allowed in the calibration.

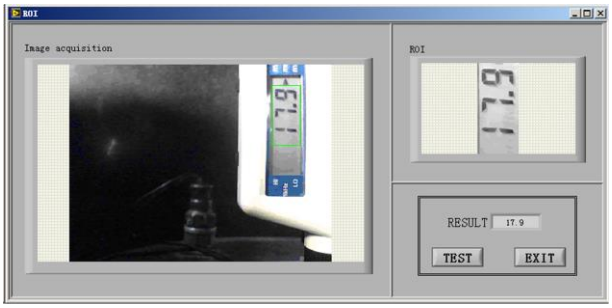

Fig. 10. Setting of ROI.

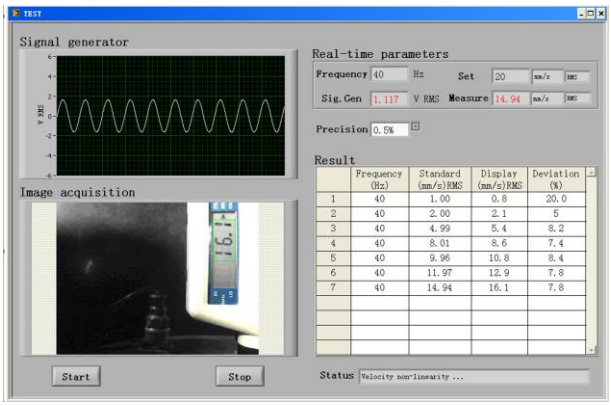

Fig. 11. Operation interface of the calibration system.

5. Conclusions

An automatic calibration system for digital-display vibrometers is proposed based on machine vision. In the system, some image processing and recognition methods for segmented digits is presented. Stroke correction has made every stroke of the characters to be recognized vertically, which leads to easier recognition of segmented-digits. The segmented-digits with decimal point have been precisely recognized according to their morphologic characteristics. Especially, the requirements of correctly recognizing vibrating digits are analyzed, which give out the permissible maximum shaking amplitude considering the acquiring speed of the digital camera, the vibration frequency, the minimum distance between the ROI border and the stroke of the characters to be identified, and the minimum distance between the strokes of the characters to be identified. The method of identifying the alternating digits is also studied, which shows that when a group of continuous display images in a relatively long period are captured and recognized respectively, and the values whose difference is not more than one resolution of the vibrometer are deemed as the same, the value that has the most occurrences is the final correct result. An alarm program is also completed to remind the operator of checking and correcting the system if a recognition error happens or an accident datum is recognized so that the deviation of the vibrometer has exceeded a preset value, which will avoid a recognition error due to the contingency. Experimental results show that the recognition rate for the digit images is about 99.75% and the calibration efficiency of digital-display vibrometers is greatly improved.

The system has been applied in a metrology station of electrical power plants in China for calibrating vibrometers automatically. Moreover, the proposed image recognition methods could be widely popularized in the circumstance where vibrating or alternating segmented-digit images should be recognized.

Table 3. Calibration results of velocity non-linearity.

f (Hz)	Standard $(mm/s)_{RMS}$	Display* $(mm/s)_{RMS}$	Deviation (%)
40	1.00	0.8 / (0.8)	20
40	2.00	2.1 / (2.1)	5
40	4.99	5.4 / (5.4)	8.2
40	8.01	8.6 / (8.6)	7.4
40	9.96	10.8 / (10.8)	8.4
40	11.97	12.9 / (12.9)	7.8
40	14.94	16.1 / (16.1)	7.8
40	19.99	21.5 / (21.5)	7.6
40	29.98	32.1 / (32.1)	7.1

*: the value outside of brackets is the recognition result and the value in the brackets is the actual display value read by naked eyes.

Table 4. Calibration results of frequency response (displacement).

f (Hz)	Standard $(\mu m)_{P-P}$	Display* $(mm)_{P-P}$	Deviation (%)
10	49.96	0.044 / (0.044)	11.9
20	50.15	0.051 / (0.051)	1.7
30	50.02	0.050 / (0.050)	0.0
40	49.79	0.049 / (0.049)	1.6
50	50.04	0.049 / (0.049)	2.1
60	49.98	0.049 / (0.049)	2.0
80	49.86	0.048 / (0.048)	3.7
100	49.78	0.049 / (0.049)	1.6
160	49.83	0.051 / (0.051)	2.3

*: the value outside of brackets is the recognition result and the value in the brackets is the actual display value read by naked eyes.

Acknowledgements

This research is sponsored by the Science Fund for Creative Research Groups of National Natural Science Foundation of China (Grant No. 51221004), the Zhejiang Provincial Science Fund for Distinguished Young Scholars in China (Grant No. LR12E05001), the National Natural Science Foundation of China (Grant No. 51375443), and the Key Science and Technology Innovation Team Program of Zhejiang Province in China (Grant No. 2009R50008).

References

[1] Payne, W.V., Geist, J. (2007). Low cost digital vibration meter. *J. Res. Natl. Inst. of Stan.*, 112(2), 115–128.

[2] Cristallia, C., Paoneb, N., Rodriguez, R.M. (2006). Mechanical fault detection of electric motors by laser vibrometer and accelerometer measurements. *Mech. Syst. Signal Pr.*, 20(6), 1350–1361.

[3] Lee, S.K., White, P.R. (1998). The enhancement of impulsive noise and vibration signals for fault detection in rotating and reciprocating machinery. *J. Sound Vib.*, 217(3), 485–505.

[4] Tandon, N., Choudhury, A. (1999). A review of vibration and acoustic measurement methods for the detection of defects in rolling element bearings. *Tribol. Int.*, 32(8), 469–480.

[5] ISO 16063-11 (1999). Methods for the calibration of vibration and shock transducers: Part 11. Primary vibration calibration by laser interferometry. International Organization for Standardization.

[6] General Administration of Quality Supervision, Inspection and Quarantine of the People's Republic of China (2000). JJG 676-2000 Working Measuring Vibration Instruments. Beijing, China: China Metrology Publishing House.

[7] He, W., Jia, S.S. (2001). Development of Automatic Vibration Calibration System. *Proceedings of the International Symposium on Precision Mechanical Measurement*. Hefei, China.

[8] Hemming, B., Fagerlund, A., Lassila, A. (2007). High-accuracy automatic machine vision based calibration of micrometers. *Meas. Sci. Technol*., 18(5), 1655–1660.

[9] Hemming, B., Lehto, H. (2002). Calibration of dial indicators using machine vision. *Meas. Sci. Technol*., 13(1), 45–49.

[10] Andria, G., Cavone, G., Fabbiano, L., Giaquinto, N., Savino, M. (2009). Automatic calibration system for digital instruments without built-in communication interface. *XIX IMEKO World Congress*. Lisbon.

[11] Alegria, F.C., Serra, A.C. (2000). Automatic calibration of analog and digital measuring instruments using computer vision. *IEEE Trans. Instrum. Meas.*, 49(1), 94–9.

[12] Alegria, F.C., Serra, A.C. (2000). Computer vision applied to the automatic calibration of measuring instruments. *Measurement*, 28(3), 185–195.

[13] Vázquez-Fernández, E., González-Jorge, H., Dacal-Nieto, Á., Martín, F., Formella, A. (2008). Human feature perception as a complementary method for digit recognition. *Conference on Visualization, Imaging, and Image Processing*. Palma de Mallorca, Spain.

[14] Vázquez-Fernández, E., Dacal-Nieto, A., González-Jorge, H.s, Martín, F., Foemella, A. and Alvarez-Valado, V. (2009). A machine vision system for the calibration of digital thermometers. *Meas. Sci. Technol*., 20(6), 1–7.

[15] Belan, P.A., Araujo, S.A., Librantz, A.F.H. (2013). Segmentation-free approaches of computer vision for automatic calibration of digital and analog instruments. *Measurement*, 46(1), 177–184.

[16] Kiwilszo, M., Zieliński, A., Smulko, J., & Darowicki, K. (2012). Improving AFM Images with Harmonic Interference by Spectral Analysis. *Microscopy and Microanalysis*, 18(01), 186–195.

[17] Samper, D., Santolaria, J., Majarena, A. C., & Aguilar, J. J. (2013). Correction of the Refraction Phenomenon in Photogrammetric Measurement Systems. *Metrology and Measurement Systems*, 20(4), 601–612.

[18] Dobosz, M., Usuda, T., Kurosawa, T. (1998). Methods for the calibration of vibration pick-ups by laser interferometry: II. Experimental verification. *Meas. Sci. Technol*., 9(2), 240–249.

[19] Gonzalez, R.C., Woods, R.E. (2008). *Digital Image Processing, Third Edition*. Upper Saddle River, New Jersey: Pearson Prentice Hall.

[20] Pastor, M., Toselli, A., & Vidal, E. (2004). Projection profile based algorithm for slant removal. *In Image Analysis and Recognition* 183–190. Springer Berlin Heidelberg.

[21] Richard, G.C., Eric, L. (1996). A Survey of methods and strategies in character segmentation. *IEEE Trans. Pattern Anal.*, 18(7), 690–706.